NASA/TM-2011-217052

Conical Shock-Strength Determination on a Low-Sonic-Boom Aircraft Model by Doppler Global Velocimetry

Gregory C. Herring and James F. Meyers
Langley Research Center, Hampton, Virginia

February 2011

NASA STI Program . . . in Profile

Since its founding, NASA has been dedicated to the advancement of aeronautics and space science. The NASA scientific and technical information (STI) program plays a key part in helping NASA maintain this important role.

The NASA STI program operates under the auspices of the Agency Chief Information Officer. It collects, organizes, provides for archiving, and disseminates NASA's STI. The NASA STI program provides access to the NASA Aeronautics and Space Database and its public interface, the NASA Technical Report Server, thus providing one of the largest collections of aeronautical and space science STI in the world. Results are published in both non-NASA channels and by NASA in the NASA STI Report Series, which includes the following report types:

- TECHNICAL PUBLICATION. Reports of completed research or a major significant phase of research that present the results of NASA programs and include extensive data or theoretical analysis. Includes compilations of significant scientific and technical data and information deemed to be of continuing reference value. NASA counterpart of peer-reviewed formal professional papers, but having less stringent limitations on manuscript length and extent of graphic presentations.

- TECHNICAL MEMORANDUM. Scientific and technical findings that are preliminary or of specialized interest, e.g., quick release reports, working papers, and bibliographies that contain minimal annotation. Does not contain extensive analysis.

- CONTRACTOR REPORT. Scientific and technical findings by NASA-sponsored contractors and grantees.

- CONFERENCE PUBLICATION. Collected papers from scientific and technical conferences, symposia, seminars, or other meetings sponsored or co-sponsored by NASA.

- SPECIAL PUBLICATION. Scientific, technical, or historical information from NASA programs, projects, and missions, often concerned with subjects having substantial public interest.

- TECHNICAL TRANSLATION. English-language translations of foreign scientific and technical material pertinent to NASA's mission.

Specialized services also include creating custom thesauri, building customized databases, and organizing and publishing research results.

For more information about the NASA STI program, see the following:

- Access the NASA STI program home page at *http://www.sti.nasa.gov*

- E-mail your question via the Internet to help@sti.nasa.gov

- Fax your question to the NASA STI Help Desk at 443-757-5803

- Phone the NASA STI Help Desk at 443-757-5802

- Write to:
  NASA STI Help Desk
  NASA Center for AeroSpace Information
  7115 Standard Drive
  Hanover, MD 21076-1320

NASA/TM-2011-217052

Conical Shock-Strength Determination on a Low-Sonic-Boom Aircraft Model by Doppler Global Velocimetry

Gregory C. Herring and James F. Meyers
Langley Research Center, Hampton, Virginia

National Aeronautics and
Space Administration

Langley Research Center
Hampton, Virginia 23681-2199

February 2011

Available from:

NASA Center for AeroSpace Information
7115 Standard Drive
Hanover, MD 21076-1320
443-757-5802

Contents

Abstract

A nonintrusive laser technique Doppler global velocimetry (DGV) was used to determine conical shock strengths on a supersonic-cruise low-boom aircraft model. The work was performed at ≈Mach 2 in the Unitary Plan Wind Tunnel. Water was added to the wind tunnel flow circuit to generate small ice particles used as flow seeding for the DGV system. DGV generates two-dimensional (2-D) maps of three components of velocity that span the oblique shock. Shock strength (i.e. fractional pressure increase) is determined from observation of the flow deflection angle across the shock in combination with the standard shock relations. Although DGV had conveniently and accurately determined shock strengths from the homogenous velocity fields behind 2-D planar shocks [Herring, Meyers, and Hart, Meas. Sci. Tech. ***20****, 045304-045313 (2009)], the inhomogeneous 3-D velocity fields behind the conical shocks presented additional challenges. Shock strength measurements for the near-field conical nose shock were demonstrated and compared with previously-published static pressure probe data for the same model in the same wind tunnel. Fair agreement was found between the two sets of results.*

1. Introduction

1.1 Background

Physical probes can sometimes perturb the measured data obtained in complicated inhomogeneous flow fields, thus biasing the quality of the measurements. To avoid this perturbation, researchers began measuring off-body flow velocities by seeding various types of small particles into the flow and measuring the Doppler shift of the Mie scattering [1-3] with laser beams. Historically particle-seeded techniques have measured only velocity, but not other flow parameters (with rare exception [4]). Hence one area of aeronautics research is concentrated on developing optical scattering and fluorescence techniques that directly probe the flow molecules to provide pressure and temperature information. While avoiding the use of particles, molecular techniques are typically expensive and labor-intensive compared to particle methods. If pressure or temperature could be derived from simpler particle-based methods, it would enhance the value of the particle methods.

Another area of aeronautics research [5] is focused on reducing sonic-boom shock strengths and noise to facilitate commercial cross-continental supersonic flights. Pressure-signature measurement in wind tunnels has long been an important aspect of predicting ground signatures and has traditionally been accomplished with pressure probes. However the probe geometry may influence the pressure data through interference with the model-induced flow field pressures. Thus optical-based noninvasive pressure measurement methods have potential to interface these two related research areas and improve the state-of-the art for shock-strength prediction and measurement.

Although shock structures can be visualized directly [6] from velocity maps determined from particle-based velocimetry techniques, in certain cases it is possible to derive pressure maps from velocity measurements. This is possible because velocity is closely related to pressure through the basic fluid dynamical relations. One rare example of deriving a pressure map from a velocity map is given in Reference 4. Recently [7] the ability of Doppler global velocimetry (DGV) to accurately measure the strengths of two-dimensional (2-D) planar shocks from a flat plate was demonstrated. Confidence in the accuracy of the measurement of Reference 7 is high because the DGV shock strength determinations were compared to another independent optical measurement: laser-induced thermal acoustics (LITA). Good agreement was found between the two optical techniques for the shock strength measurements; furthermore, the LITA technique was previously compared to and found to agree with static pressure probes in a simple homogeneous freestream flow [8].

1.2 Present Work

With this successful measurement of a planar shock strength in hand, in this report the DGV approach of Reference 7 is extended to the measurement of conical shock strength in the 3-D flowfield of a lifting body. No physical probe is required for the DGV measurement. DGV is a technique [3, 9-13] that uses a single laser beam formed into a sheet to measure three components of flow velocity at multiple locations within the 2-D laser sheet. If the laser sheet is located across a shock and oriented transverse to the shock, the measured velocity map can be used to determine the pressure increase across

the shock within the velocity map. The spatially-resolved map of flow velocity is used to determine the flow-deflection angle across the shock with about the same spatial resolution as that of the velocity map. Then the oblique and normal shock relations can be used to determine the pressure rise across the shock.

This report discusses only the DGV measured nose shock strength versus downstream location. The entire longitudinal pressure profile across the full shock structure (as is traditionally produced by translating a pressure probe) of the model was not measured with DGV due to the orientation of the light sheet set to measure the cross-flow velocity field below the model. The DGV measured nose shock data are compared to traditional static-pressure probe data for the same model in the same wind tunnel with approximately the same flow conditions [Mach 2 in the Unitary Plan Wind tunnel (UPWT) at NASA's Langley Research Center (LaRC)].

Particle image velocimetry (PIV) and laser Doppler anemometry (LDA) would not work as well as DGV with this approach because the larger particles required by these techniques would suffer significant velocity lag when traversing the shock. This would greatly reduce the spatial resolution of the measurement and offset the physical location of the shock from its actual location. In the UPWT, the condensed water seed particles are ~ 10 nm [14].

2. Methods and Experimental Setup

2.1 Velocity Measurement

Descriptions of DGV are found in the literature [3, 9-13]. The frequency of a single-longitudinal-mode Ar-ion cw laser is tuned to the peak absorption of an I_2 transition near 514 nm. The laser is actively locked to the side of the I_2 transition to stabilize the frequency drift of the laser. This is accomplished by passing a small fraction of the laser beam through a Bragg cell and shifting the wavelength to a position ½ way down the absorption profile. Then the Bragg shifted beam is passed through a vapor-limited I_2 vapor cell (the first of two in the setup) and the absorption signal is used to control the laser frequency in an active feedback loop. The remaining laser beam power is formed into a sheet (~ 200 μm thickness) to define a planar interrogation region in the test section. In this supersonic flow, Rayleigh scatter from ice particles passing through

the laser sheet is collected by three fiber-optic probes placed to observe the light sheet from three different directions (one probe per velocity component). The collected light from all three probes is passed to a single receiver system which splits the light into two portions, part impinging directly on a cooled-CCD camera (reference) and the remaining passing through the second vapor-limited I_2 vapor cell to a second CCD camera (signal). The three normalized (= signal / reference) amplitude maps are converted to Doppler shift maps from the known I_2 absorption. Based on the optical geometries, the Doppler shifts are then related to the velocity of the ice particles.

In the present measurement scheme the laser light sheet was located in the vertical plane and projected across the test section from a side window. The fiber optic probes were located at the far corners of the test section window to maximize geometric accuracy when converting the three non-orthogonal velocity measurements to the standard orthogonal coordinate system. Thus the technique measures the three components of velocity simultaneously with a spatial resolution of 0.2 mm covering a region 225 by 150-mm in the center of the test section.

In the present work, ≈ 3 liters of liquid H_2O were added to the wind tunnel circuit to obtain a flow humidity equivalent to a dew point (DP) of about - 12 °C. Water condensation in the tunnel nozzle generates a fog of ice crystals in the cold freestream flow to produce the needed scattered laser light. The ~ 10-nm particle size insures particle-tracking fidelity of the flow. Light scatter from these small particles is in the Rayleigh regime rather than the Mie regime. Multiple scattering effects were assumed to be minimal, and thus no check or correction for these effects was made. Translating the model along the axial direction through the fixed vertical light sheet produced the series of measurement planes at various distances downstream of the model nose. All measurement ensembles consisted of 50 sequential image pairs, each with an exposure integration time of 1 sec, yielding an averaged measurement over 60 sec. Additional details of the DGV test were described previously [7, 15].

2.2 Shock Strength Determination

The objective of the present work was to determine the pressure change across a conical shock wave based on maps of cross-flow velocity. The velocity measurements

used in this study were previously reported [15]. If a velocity map spans an oblique shock, then the flow-deflection angle, α, behind the shock can be determined. Once a change in the flow velocity vector was measured, the ideal shock relations (found in many textbooks and reports, e.g., [16]) were used to calculate the change in pressure across the shock. Using the same six-step process reported in [7], both oblique and normal shock relations were needed to convert from velocity to pressure information.

Velocity vector measurements before and behind the shock provide the angular change, α, in the flow direction across the shock. The oblique-shock relations, along with the incoming freestream Mach number, M_1, and α, were then used to determine a unique shock angle θ_1. A unique θ_1 determines the normal component M_{1N} (relative to the shock front at that particular location) of the incoming Mach number. Lastly, the normal-shock relations determine the fractional pressure increase across the shock using this normal component of M_1.

Note that the conical shock relations are not used in this approach because the model is not an infinitely long cone. Behind a conical shock a 3-D flow exists. As the measurement location moves from the shock towards the conical surface (equivalent to moving downstream), the flow angle continuously deflects towards the surface as the flow is compressed. In the present work on this low-boom aircraft model with its very slender form, the shock angle is predominately determined by the incoming Mach number and adopts characteristics more similar to a true Mach wave rather than those of the ideal semi-infinite cone case of the conical shock tables. The present approach to measuring shock strength determines the flow deflection angle as close to the shock as possible, where the oblique shock relations hold and give the shock angle. Refer to Section 4 for a discussion of a correction to the raw measurement due to the fact that the spatial smoothing of the shock location by the modulation transfer function of the small lenses used by the DGV optical system prohibited the measurement of the flow deflection angle immediately behind the conical shock.

In summary, shock strengths are determined from velocity maps as follows:

(1) Measure (or assume from known wind tunnel conditions) incoming freestream axial velocity and Mach number.

(2) Measure change in transverse velocity across the shock.

(3) Determine flow deflection angle α = ARCTAN ($\Delta V_{transverse}$ / $V_{streamwise}$).

(4) Use oblique shock tables to determine shock angle relative to incoming flow.

(5) Use trigonometry to determine normal component of incoming flow relative to shock.

(6) Use the normal component of the incoming freestream flow and the normal shock tables to determine ratio of pressures and ratio of temperatures across the shock.

Measurement of the temperature change across the shock is equally feasible with the same approach as for pressure. In addition, pressure decreases across expansion fans are also obtainable by an analogous method [7]. For expansions, M_1 is used with the measured flow-deflection angle to determine the Mach number M_2 behind the expansion with the Prandtl-Meyer flow equations [16]. Then M_1 / M_2 determines the pressure and temperature changes according to the isentropic flow relations [16].

2.3 Wind Tunnel and Low-Boom Model

All measurements were made in test-section 1 of the UPWT at LaRC. A 1/160 scale model (designed for a low boom at supersonic cruise) was installed in the 1.2 by 1.2-meter test section and used to generate a near-field sonic boom profile. Additional details of the wind tunnel [17] and the low-boom aircraft model [18-20] are available. The fuselage was oriented at zero degrees angle-of-attack (AOA), while the wing AOA was slightly positive which provided a net lift (i.e., the trailing edge of the wings are angles slightly downward relative to the fuselage). The model length, L_e, was 9.0 inch, and the full wing span, b, was 4.5 inch. Additional details of the model are presented in References 19 and 20.

The present work was performed with a standard Mach number 1.97 airflow (velocity = 535 m/sec), a free-steam static pressure of 7.6 kPa, and a freestream static temperature of 183 K. However a reduced freestream Mach number = 1.90 (and an increased freestream static temperature of 190 K) was used in analyzing the present DGV data to account for the addition of significant water to the wind tunnel circuit. Condensation of the water vapor into ice crystals in the nozzle slightly heats the flow, reducing the Mach number and absolute velocity, while increasing static temperature and sound speed [17, 21].

A schematic of the locations of the DGV and pressure probe measurements is shown in the side-view of Figure 1. The vertical thick dashed lines indicate five of the many DGV measurement planes at a variety of distances downstream of the nose. The single horizontal thick dashed line indicates the line of traverse for the probe measurements, which is roughly parallel to the centerlines of both the tunnel and model. The thin dotted line indicates the general shock structure. A photograph of a silhouette of the model installed in the test section against the green laser light sheet is shown in Figure 2. The DGV and pressure probe measurements were made sequentially, separated by a few years, and thus the model had been removed and reinstalled between the two tests.

3. Results

3.1 DGV Velocity Profiles

Figure 3 shows a typical measured two-dimensional velocity map from Reference 15 of crossflow velocity (Y component = V), where color gives the magnitude of the transverse velocity component over the range -10 to +10 m/sec. The velocity scale is given by the reference color bar in the lower right portion of the green shaded area. The plane of the map is orthogonal to the freestream direction X and is located 1.39 model lengths (12.5 inch) downstream of the nose tip. To determine the pressure change at a given downstream location, the transverse velocity profile along the Y direction (indicated by arrowed red line) is used to obtain the change in transverse velocity component. Moving outward from the model along the red line indicates larger values of Y, the transverse distance away from the model (below the model). Note at this far downstream location, the nose shock is no longer observable along the red line because the nose shock has expanded beyond the limits of the velocity map. However the nose shock is observable in the lower-right portion of the velocity map passing through the color bar as the curved transition from the freestream green to the faint yellow behind the shock. At further upstream locations, the nose shock is easily identifiable along the red line and is used to determine the nose shock strengths at these upstream locations. The variable Y in this report is equivalent to the variable h in References 19 and 20.

The far-downstream location of Figure 3 was not chosen as an example of a map used to determine nose shock data, but to illustrate the major features of the flow field behind the model. Although these features may be identified with vapor screen visualization, Figure 2, only their location can be determined. For example, the nose shock cannot be seen in Figure 2, but the wing-tip vortices and shock structures generated by the wing can be located. DGV provides quantitative measures of these structures. For example the velocity patterns from the two counter rotating wing-tip vortices are found by the two blue circles coupled with corresponding red circles (portions of the red circles close to the model are lost due to laser flare from the model) showing the typical cross-flow patterns of a vortical flow. The red crescent to the right of the model indicates a high cross-flow velocity pattern moving away from the model. The corresponding blue crescent sections show the second half of the typical sonic "N" velocity pattern. These patterns not only show the location of these structures, but their strength. For example, the results indicate that the strength of the shock generated by the wing is greater at 45-degrees than directly below the model.

At locations further upstream, typical transverse velocity profiles and axial freestream velocities are shown in Figure 4. Two velocity profiles across the nose shock region are shown for four different downstream locations (3.5, 4.0, 4.5, and 5.0 inch from the nose tip). The axial freestream velocity (U component along the X axis) is read off the left vertical scale, while the transverse velocity (V component along the Y axis) is read off the right vertical axis. Each transverse and freestream velocity profile is taken from a single line of velocity data (along the equivalent red line illustrated in Figure 3). The upper set of four curves in Figure 4 that are approximately flat show (from 3 to 8 inch) profiles of the freestream velocity U for four downstream locations, while the lower set of four curves show profiles of the transverse velocity V. The upper red curve of axial velocity corresponds to the lower red curve of transverse velocity. This convention applies to each of the four colors. These V components show a clear increase in velocity at about Y = 3-4 inch downstream (i.e. shock location) as you move further below the model and across the oblique shock. The flow-deflection angle α at the oblique shock at each downstream location is determined from these measured velocity profiles according to α = ARCTAN (change in transverse velocity across shock / freestream velocity before

shock) = ARCTAN (ΔV / U). The additional increase in velocity at the extreme left hand side (Y =1-2 inch region) of the V components is an artificial effect due to the unwanted scattered laser light (flare) from the model.

Shock angles θ_1 can then be determined from the flow turning angles α and the oblique shock tables as in Reference 7. Shock angles determined from the flow-deflection angles are plotted in Figure 5, as a function of distance downstream of the model nose. Figure 5 shows 23 separate determinations of shock angle from corresponding flow deflection angles, which were derived from velocity maps (each averaged over 60 sec). Data is shown from two days (March 16 [yellow triangles] and 17 [pink squares]), where the model was rotated 180 degrees on March 17 with respect to the orientation of March 16. The smooth connection between the two different days of data illustrates the strong internal consistency (i.e. precision), of the DGV data, but does not make any clear statement about the absolute accuracy.

The flow-deflection angles from localized spatial regions used to produce these localized shock angles θ_1, i.e. the yellow and pink data of Figure 5, can be checked by comparing with a somewhat independent determination of shock angle θ_A by further averaging over more extended spatial regions. This second method of determining shock angle comes from observing the vertical shock location in each of the DGV transverse velocity maps at many downstream locations. These measured shock locations are synthesized into the single plot of Figure 6, which effectively shows a 2-D illustration of the shock in a single streamwise plane that intersects the model centerline. Several quasi-independent maps of shock position obtained over the four days of testing are shown in Figure 6. Each color shows the result of a single test (i.e. a single morning or afternoon wind tunnel run) where the DGV sheet position was changed about 7-8 times over the approximate two-hour period during that particular test run. As noted before, on some days, the model was rotated 180 deg with respect to other days.

The shock angles θ_A for each individual run (i.e. each color) of Figure 6 are determined from θ_A = ARCTAN (slope) = ARCTAN (ΔY / ΔX) and are also plotted on Figure 5 as blue diamonds. The solid black line of Figure 5 is a power-law fit to the blue diamonds. Each blue diamond of Figure 5 is from one run (i.e. one color) from Figure 6. These angles over extended spatial averages are in fair agreement with the locally-

determined angles (yellow triangles and pink squares), but clearly the numbers and trends are slightly different. This slight disagreement shows the advantage of the local averages in determining spatially-resolved shock angles when the shock is not perfectly straight. Both data sets (locally and extended averages) of Figure 5 are essentially showing a slight curvature of the conical shock, and the uncertainties for the extended averages are likely more affected by this shock curvature. In the discussion below, only the locally averaged shock angles (yellow and pink data of Figure 5) are used to determine the DGV-based shock strengths.

3.2 Nose Shock Strength

Figure 7 shows a summary of previously measured nose shock strength as a function of distance downstream of the model. The solid blue diamonds are the raw static pressure probe data (read from Figures 14-17 of Reference 19 and from Figures 16-17 of Reference 20), while the open yellow diamonds show the probe data after the original authors have corrected the raw data (read from Figure 9 of Reference 19 and Figure 13 of Reference 20). Reference 19 and 20 discuss the method and reasons (e.g. smearing of the shock profile due to model vibration) for these corrections. In this report, the corrected probe data (open yellow diamonds) are taken as the final probe data for the purpose of comparison to DGV.

Local shock angles (yellow and pink data of Figure 5) are used to deduce DGV shock strength (fractional pressure change = dP / P) using the oblique and normal shock tables as in Reference 7. Raw shock strength determination is shown in Figure 7 from two days of testing (March 16 and 17), where the model orientation was rotated 180 degrees on March 17 with respect to that of March 16. The raw DGV shock strength data is about 50% smaller than the corrected pressure probe data. The open black triangles show both days of DGV data after a correction (described below in Section 4) because the measured flow deflection angles are obtained at a small finite distance downstream of the shock (not immediately after the shock). After correction of the DGV data, the DGV and the probe data are in modest but not perfect agreement. Near the 20-inch downstream location, the corrected DGV results are about 20% smaller than the corrected probe results. However the laser technique is nonintrusive and can be used to measure

further upstream and closer to the model nose tip than the probe. The probe measurements were terminated at the x ≈ 15-inch location to avoid interferences between the probe and the model. Table 1 shows the numerical values used in Figure 7.

Figure 8 shows the same data as shown in Figure 7, but plotted as normalized pressure change across the shock as a function of span-normalized distance downstream. The abscissa of this normalized plot (typically used in the sonic boom community) is called the far-field parameter and gives a shock strength value as if the pressure signature has fully evolved into the N-wave shape, even though a low-sonic-boom signature never reaches an N-wave shape. The normalized far field shock strength is of interest in minimizing sonic boom strengths on the ground and usually becomes constant as a function of distance away from the vehicle or model. This far-field asymptote from Reference 20 (based on Whitham theory [22]) is shown with a horizontal dashed line.

4. Discussion

4.1 Correction to Raw DGV Determinations of Shock Strength

In the freestream, the mean free path is ~ 10^{-5} cm, and the shock thickness is expected to be of the order of a few mean free paths. But the velocity profiles in Figure 4 do not show sharp jumps in velocity over the shock as almost certainly must occur in reality. The apparent shock thickness in Figure 4 is ~ 2 cm (i.e. ~ 1 inch) and is artificial. This is because the imaging optics of the apparatus consist of 5 mm diameter collection lenses (mounted on the ends of optical fibers) located about ¾ of a meter away from the laser light sheet. The limited numerical aperture of the light collection optics gives a finite modulation transfer function (MTF), i.e. limited spatial resolution. This optical arrangement and the MTF are dictated by the limited optical access to the test section as restricted by the window supporting structures on the outside of the test section. These structures prohibited the use of larger diameter lenses that would yield sharper images, to view the measurement plane. Thus the smoothing effect of the small lenses did not allow the determination of the transverse velocity immediately behind the shock, but the velocity could be determined approximately 1-inch downstream.

The same problem was encountered in the previous work of Reference 7, where the measurement of shock strengths for two-dimensional planar shocks was demonstrated

on a flat plate with the same DGV apparatus. However in the previous work, the flow behind the planar shock was uniform (i.e. no compression and change in flow direction after the crossing the planar shock) and it did not matter if the finite MTF and artificially large shock thickness forced a measurement of the post shock velocity a small finite distance downstream from the shock. In fact the uniform flow behind the shock proved to be an advantage in that work.

Figure 9 shows examples of the transverse velocity profiles as a function of distance above a flat plate from Reference 7. The flow is effectively from right to left. These transverse velocity profiles were used to determine shock strengths from oblique planar shocks. The uniform flow (constant velocity) behind the shock is illustrated at several downstream locations relative to the leading edge of the plate. There is little uncertainty about the velocity values in front of and behind the planar shocks. This contributed to the excellent results of shock and expansion strengths derived from DGV that compared well to LITA. Although the well-behaved velocity profiles of Figure 9 are not used here, they are presented for comparison with the profiles of Figure 4 for the present conical shocks.

In contrast, the shocks in the velocity profiles in Figure 4 are less well defined because (1) flare from the model has not been completely removed from the signal and (2) the flow behind the conical shocks is 3-dimensional. In the case of an infinitely long cone, the flow behind the conical shock would be slowly compressed and turned towards the cone as the flow progress downstream. If one measures the transverse velocity 1 inch downstream of the shock (which must be done due to the finite MTF), the effect of the flow direction change between the shock and the measurement point must be accounted for in order to derive the flow direction immediately behind the shock. Thus the raw flow angle measurements that are made 1 inch downstream of the conical shocks must be corrected to reflect the value immediately behind the shock.

Following the scheme presented in Reference 23, Figure 10 illustrates the geometry and physical basis of correction. In order to make this correction, one must know the nature of the flow between the measurement point P and the shock (point E on the same streamline as point P). If measuring shocks far downstream of the model (by many body lengths), then approximating the conical shock as a true Mach wave (i.e. an

extremely weak shock) rather than a typical oblique weak shock would be reasonable. In this case, the correction would be zero. If measuring far upstream (i.e. upstream of the data presented in Figure 7 where the initial cone shape of the model nose has not yet changed to a typical constant-diameter fuselage), then an infinite cone approximation would be reasonable and the conical shock tables could be used for the correction. The flow under investigation is in-between these two situations, where Figure 7 shows DGV data for shock strength from about 0.5 to 2 body lengths downstream of the model nose tip. It is assumed that the flow between the measurement point and the shock is described by a generic slender 2-D airfoil as in Figure 10.

The flow over the airfoil, immediately after the conical shock and above the model, begins by being directed maximally upward, but slowly turns downwards as one moves downstream until midway between the nose shock and the tail shock where the flow direction regains its original horizontal direction. This downward deflection of the flow, due to the slight and gradual compression behind the shock, is a reasonable approximation until reaching the general location of the tail shock.

The transverse velocity change cannot be determined upstream of point P in Figure 10 because of the finite MTF in the DGV optical system. This is about 38% of the distance downstream (i.e. 1 inch downstream of the shock) between the nose shock and the midpoint of the nose and tail shocks. First, approximating a flow path streamline as a parabola (dashed line and bold arrows in Figure 10) in the region between the nose and tail shocks, the flow direction is expected to regain its horizontal attitude at the midpoint between the nose and tail shocks. Second the flow angle change between the shock and the midpoint is approximated to be linear. With these approximations, the flow direction has changed downward by about $1 / (1-0.38) = 1.62 \approx 60\%$ between the shock and the measurement point. Adjusting the measured flow directions by this 60% and then determining the shock strengths, produces the corrected data points (black color) of Figures 7 and 8. These corrected data show better agreement with the corrected probe measurements, but may be starting to diverge from the probe results near the 20-inch downstream location.

4.2 Uncertainties for DGV-Based Shock Strength

The spread in the DGV data of Figures 7 and 8 (relative to an imaginary smooth curve fit through the data) suggests that the statistical uncertainty (precision) is about $\pm$ 10% for a single time-averaged (60 sec) measurement of shock strength. Estimating the systematic uncertainty (accuracy) is more difficult due to the 60% correction that has to be made to the current raw measurements. In addition, the lack of confident comparison benchmarks also contributes to the lack of information necessary to access the accuracy. In other words, how accurate are the probes? Assuming that the corrected pressure probe measurements of Figures 7 and 8 are truly correct, one might estimate that the DGV results are trending approximately 20% low for the last three points near the 20-inch downstream location. Thus the systematic uncertainty in the DGV method is estimated to be $\leq$ 20%.

Although unlikely (partially because the probe results are corrected by only ~ 20% and the DGV results are corrected by ~ 60%), it is possible that the DGV results are more accurate than the probe results. See References 18-20 for a discussion on the uncertainties of the pressure probe measurements. Note that in Reference 7, the DGV results agreed with another optical method (LITA) to within a few per cent (normalized to the absolute pressure) for shock strength measurements. However in that work, the DGV raw data did not require the 60% correction that was needed in the present work.

5. Summary

DGV was used to study conical shock strengths on a supersonic-cruise low-boom aircraft model by measuring and mapping off-body flow velocity. The non-uniform nature of the velocity field and the limited MTF effectively forced a velocity measurement slightly downstream of the shock position. This presented a challenge for accurately converting the DGV velocity map to pressure change, requiring a correction to the raw shock determinations.

Near-field determinations of the shock strength across the nose shock (in the region where the shock is still ~ axially symmetric) were made from the velocity maps and compared favorably with static pressure probe data. At $\approx$ 2 body lengths downstream the DGV values are trending $\approx$ 20% lower than the probe values. This comparison

provides confidence in the ability of the laser technique to quantitatively measure shock strengths where the flow between the shock and the measurement point is well known (or alternatively for cases where one can measure the flow angle immediately behind the shock). Flows more complicated than the one studied here will present additional challenges for the successful use of this method.

Two advantages of the laser-based method are its nonintrusive nature and its ability to measure further upstream towards the apex of the conical shock in a region where the probe is not used because of probe-model interferences. Each of the two techniques has to correct its respective raw measurement (pressure probe by ≈ 20% and DGV by ≈ 60%) for a smearing of the sharp shock feature. However the physical basis of the smearing and corresponding correction is different for each technique, arguing for the reality of the general agreement of the two methods.

6. Acknowledgements

The authors thank A. A. Cavone, M. T. Fletcher, and J. W. Lee for assembly and operation of the laser apparatus and R. J. Mack and L. M. Weinstein for helpful discussions.

7. References

[1] Hunter, Jr. W W and Foughner, Jr. J T, editors 1982 Flow visualization and laser velocimetry for wind tunnels, *NASA Report CP-2243*

[2] Yeh Y and Cummins H Z 1964 Localized fluid flow measurements with an He-Ne laser spectrometer, *Appl. Phys. Lett.* **4** 176-178

[3] Samimy M and Wernet M P 2000 Review of planar multiple-component velocimetry in high-speed flows, *AIAA Journal* **38** 553-574

[4] van Oudheusden B W, Scarano F, Roosenboom E W M, Casimiri E W F, and Souverein L J 2007 Evaluation of integral forces and pressure fields from planar velocity data for incompressible and compressible flows, *Exp. Fluids* **43** 153-162

[5] Aronstein D C and Schueler K L 2005 Two supersonic business aircraft conceptual designs, with and without sonic boom constraint, *J. of Aircraft* **42** 775-786

[6] Murphy M. J. and Adrian R. J. 2007 Particle response to shock waves in solids: dynamic witness plate/PIV method for detonations, *Exp. Fluids* **43** 163-171

[7] Herring G. C., Meyers J. F., and Hart, R. C., 2009 Shock-strength determination with seeded and seedless laser methods, *Meas. Sci. Tech.* **20** 045304-045-313

[8] Hart R C, Herring G C, & Balla R J 2007 Pressure measurement in supersonic airflow by differential absorptive laser-induced thermal acoustics, *Opt. Lett.* **32** 1689-1691

[9] Elliot G S and Beutner T J 1999 Molecular filter based planar Doppler velocimetry, *Prog. Aerosp. Sci.* **35** 799-845

[10] Willert C, Stockhausen G, Klinner J, Lempereur C, Barricau P, Loiret P, and Raynal J C 2007 Performance and accuracy investigations of two Doppler global velocimetry systems applied in parallel, *Meas. Sci. Tech.* **18** 2504-2512

[11] Meyers J F 1995 Development of Doppler Global Velocimetry as a Flow Diagnostics Tool. Measurement in Fluids and Combustion Systems, Special Issue, *Meas. Sci. Tech.* **6** 769-783

[12] Meyers J F, Lee J W, and Cavone, A A 2007 Doppler Global Velocimetry *Springer Handbook of Experimental Fluid Mechanics*, Ed: C. Tropea, A. L. Yarin, and J. F. Foss (Springer-Verlag, Berlin) Chapter 5.3.4.

[13] Meyers J F 1992 Doppler Global Velocimetry - The Next Generation? *AIAA 17th Aerospace Ground Testing Conference*, Nashville, TN (July 6-8) Paper 92-3897

[14] Benedict L H, Griffith W C, Yanta W J, Spring III W C, and Boyd C F 1991 Quantification of vapor screen analysis, *AIAA 22nd Fluid Dynamics, Plasma Dynamics, and Lasers Conference*, Honolulu, Hawaii (June 24-26) Paper 91-1691

[15] Meyers J F, Lee J W, Fletcher M T, Cavone A, Viramontes J A G 2006 Supersonic flow field investigations using a fiber-optic based Doppler global velocimeter, *13th International Symposium on Applications of Laser Techniques to Fluid Mechanics* Lisbon, Portugal, (June 26-29) Paper 1019

[16] AMES Research Staff 1953 Equations, tables, and charts for compressible flow, *NASA NACA Report-1135*

[17] Jackson C M, Jr., Corlett W A, and Monta W J 1981 Description and calibration of the Langley unitary plan wind tunnel, *NASA Report TP-1905*

[18] Mack R J 2003 A supersonic-cruise business jet concept designed for low sonic boom, *NASA Report TM-2003-21443*

[19] Mack R J and Kuhn N 2004 Determination of extrapolation distance with measured pressure signatures from two low-boom models, *NASA Report TM-2004-213264*

[20] Mack R J and Kuhn N 2006 Determination of extrapolation distance with pressure signatures measured from two to twenty span lengths from two low-boom models, *NASA Report TM-2006-214524*

[21] Herring G C 2008 Mach-number measurement with laser and pressure probes in humid supersonic flow, *AIAA Journal*, **46**, 2107-2109

[22] Whitham G B 1952 The flow pattern of a supersonic projectile, *Communications on Pure and Applied Mathematics,* **5**, 301-348

[23] Thompson P A 1972 *Compressible-Fluid Dynamics,* 1st ed., (New York, McGraw-Hill) pp. 262 Chapter 5

Table 1

Method and Date or Reference	Distance Downstream (inch)	Raw DGV Flow Turn Angle (deg)	Raw DGV Shock Strength	Corrected DGV Flow Turn Angle (deg)	Corrected DGV Shock Strength	Raw Probe Shock Strength	Corrected Probe Shock Strength
DGV 3/17	1.8	0.618	0.036	1.001	0.059		
DGV 3/17	2.3	0.528	0.031	0.855	0.050		
DGV 3/17	2.8	0.449	0.026	0.728	0.043		
DGV 3/17	3.3	0.506	0.030	0.819	0.048		
DGV 3/17	3.8	0.392	0.023	0.634	0.037		
DGV 3/17	4.3	0.415	0.024	0.672	0.040		
DGV 3/17	4.8	0.392	0.023	0.634	0.037		
DGV 3/17	5.3	0.414	0.024	0.671	0.039		
DGV 3/17	5.8	0.346	0.020	0.561	0.033		
DGV 3/17	6.3	0.336	0.020	0.544	0.032		
DGV 3/17	6.8	0.336	0.020	0.545	0.032		
DGV 3/17	7.3	0.282	0.017	0.457	0.027		
DGV 3/17	7.8	0.338	0.020	0.547	0.032		
DGV 3/17	8.3	0.293	0.017	0.474	0.028		
DGV 3/16	9.3	0.281	0.017	0.455	0.027		
DGV 3/16	10.3	0.226	0.013	0.366	0.022		
DGV 3/16	11.3	0.281	0.017	0.455	0.027		
DGV 3/16	12.3	0.225	0.013	0.364	0.021		
DGV 3/16	13.3	0.203	0.012	0.328	0.019		
DGV 3/16	14.3	0.225	0.013	0.365	0.021		
DGV 3/16	15.3	0.169	0.010	0.274	0.016		
DGV 3/16	16.3	0.170	0.010	0.276	0.016		
DGV 3/16	17.3	0.148	0.009	0.240	0.014		
Probe [19, 20]	14.1					0.0210	0.0240
Probe [19, 20]	21.2					0.0140	0.0199
Probe [19, 20]	28.3					0.0140	0.0172
Probe [19, 20]	35.3					0.0110	0.0141
Probe [19, 20]	70.6					0.0060	0.0069
Probe [19, 20]	106					0.0047	0.0054

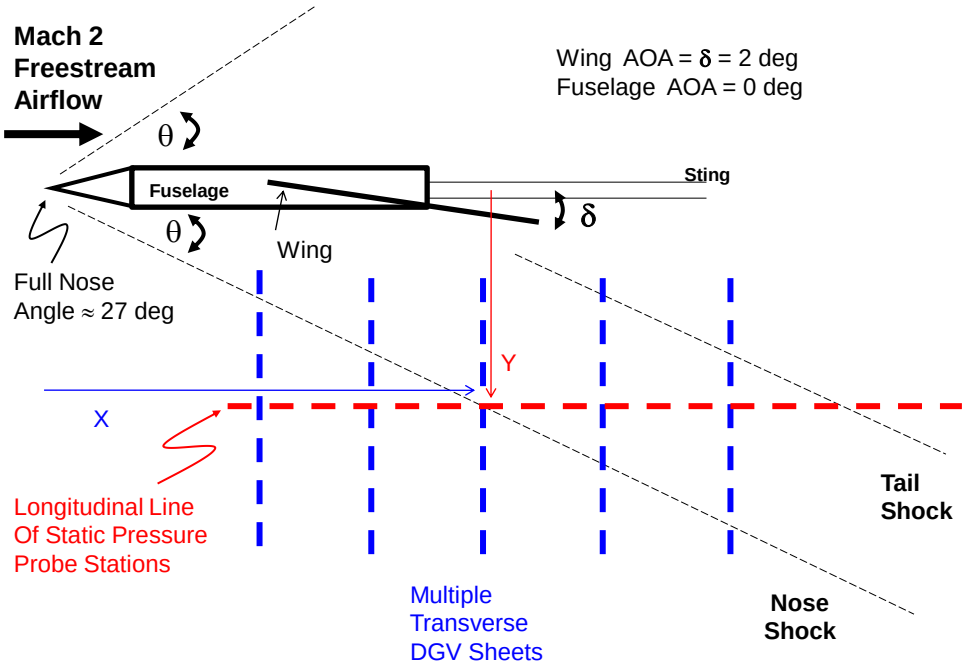

Figure 1 Side-view schematic of test setup, showing model, nose and tail shocks (thin black dashed lines), five representative light sheet locations (vertical blue heavy dashed lines indicate laser sheets transverse to freestream direction) and pressure probe locations (heavy red horizontal dashed line parallel to tunnel centerline). Fuselage AOA = zero.

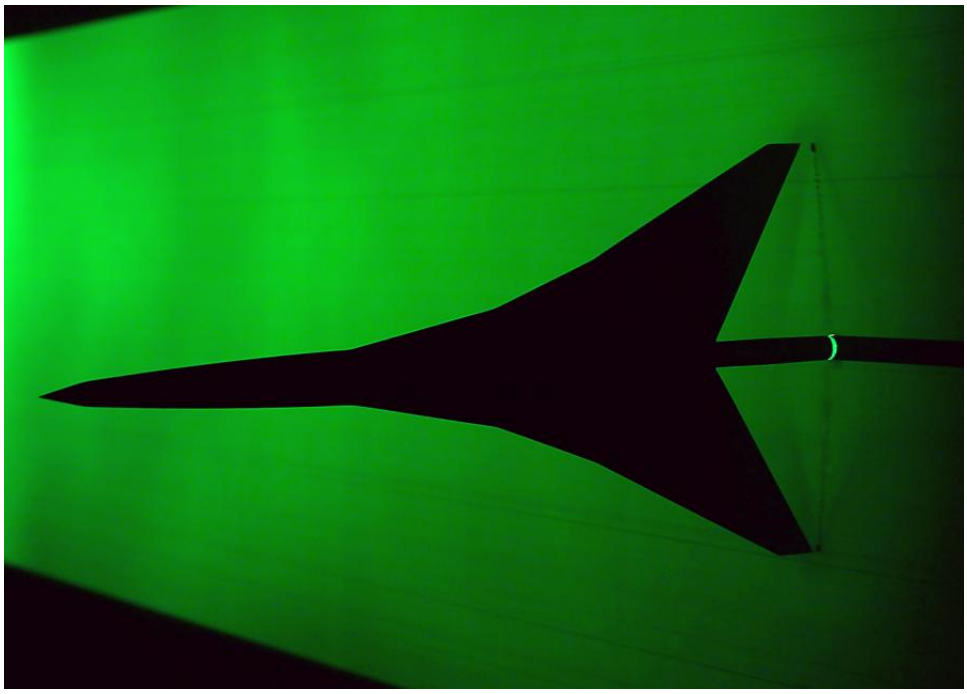

Figure 2 Top-view photograph of low-boom model installed in the UPWT in front of green laser light sheet.

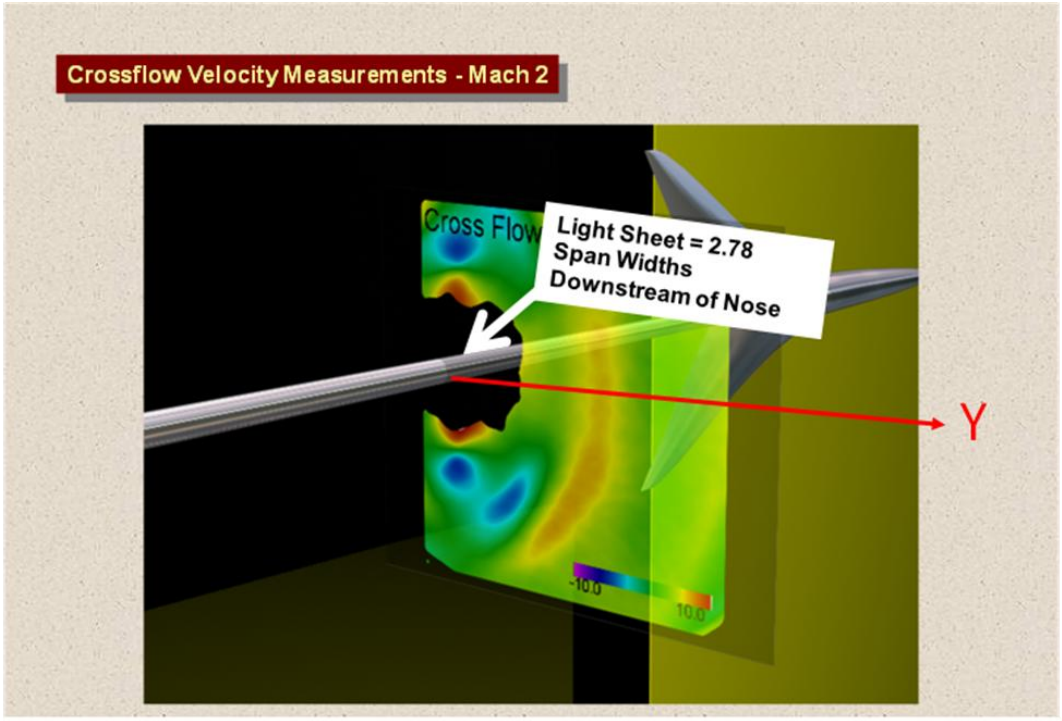

Figure 3 2-D transverse map of measured transverse velocity component V at 1.39 times the model length (= 2.78 span widths) downstream from the nose. Color indicates transverse velocity component defined by the calibration bar at lower right (units = m/sec).

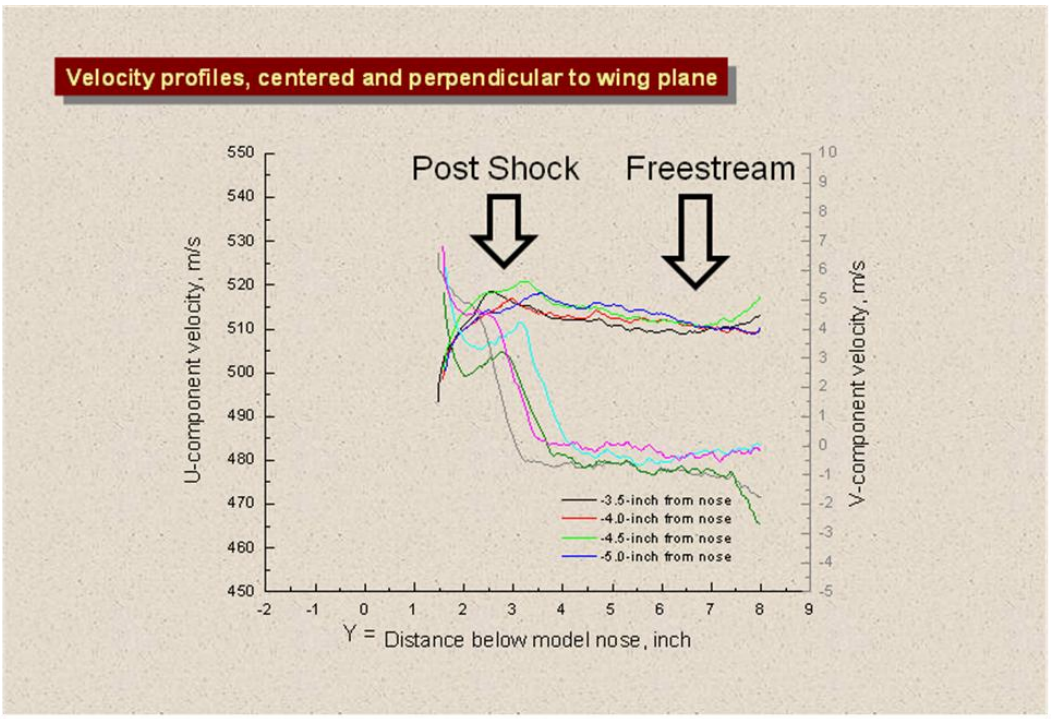

Figure 4 Axial velocity U (upper set of four approximately flat curves read on left vertical scale) and transverse velocity V (lower set of four rising curves read on right vertical scale) at four different downstream locations.

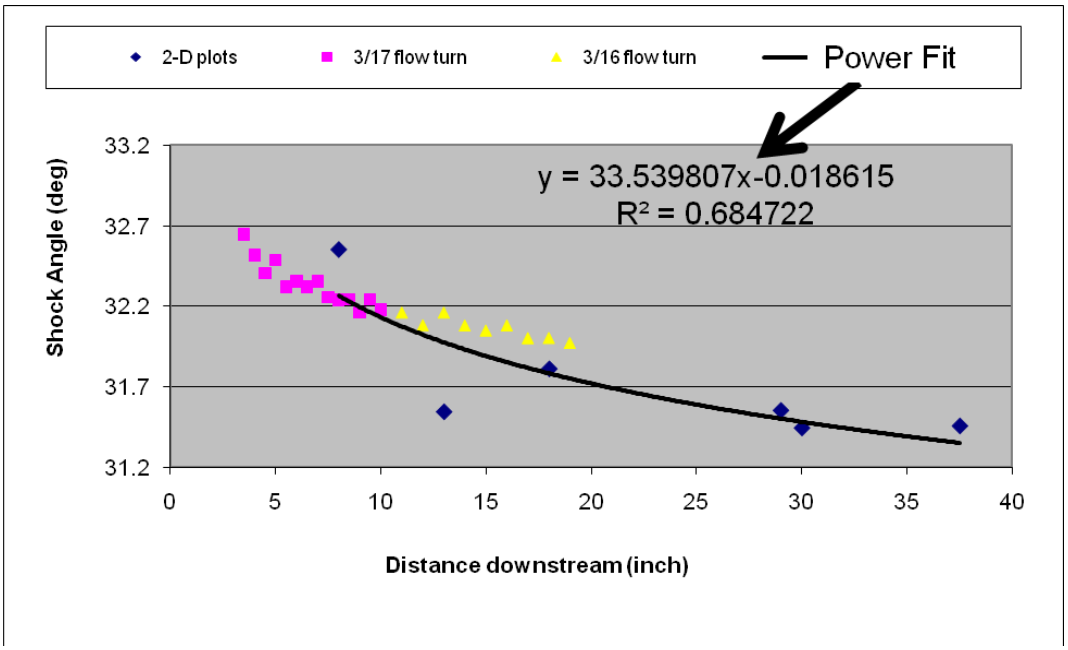

Figure 5 Shock angles θ_1 determined from flow-deflection angles from single 60-sec temporally averaged measurements from two different days, March 16 (yellow triangles) and 17 (pink squares). A second method for determining shock angles θ_A (blue diamonds) is from extended spatially averaged 2-D shock location maps from Figure 6. The solid line is a power law fit to only the blue diamonds.

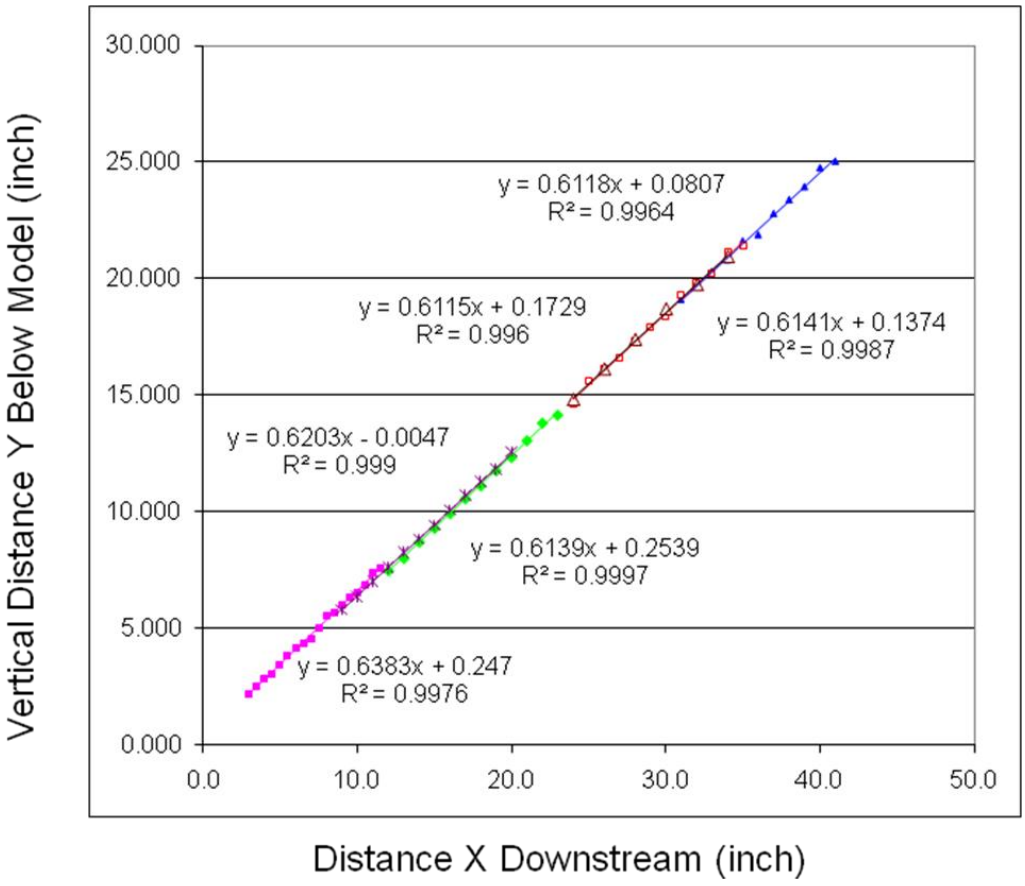

Figure 6 2-D maps of shock location used to determine spatially averaged shock angles θ_A (blue diamonds in Figure 5). Each blue diamond in Figure 5 comes from the arctangent of the slope of one colored data set here, where Y is the vertical shock location as a function of downstream distance X.

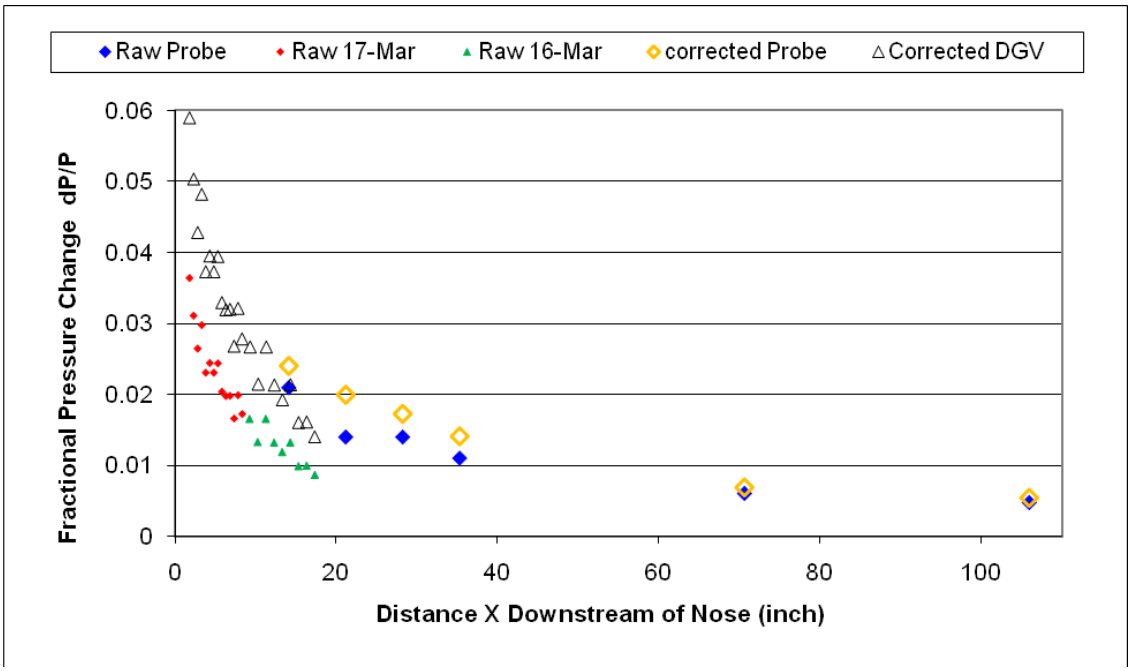

Figure 7 Comparison of nose shock strength determined from DGV on two days (March 16 and 17) and from static pressure probes [19, 20] at various distances downstream of the model nose.

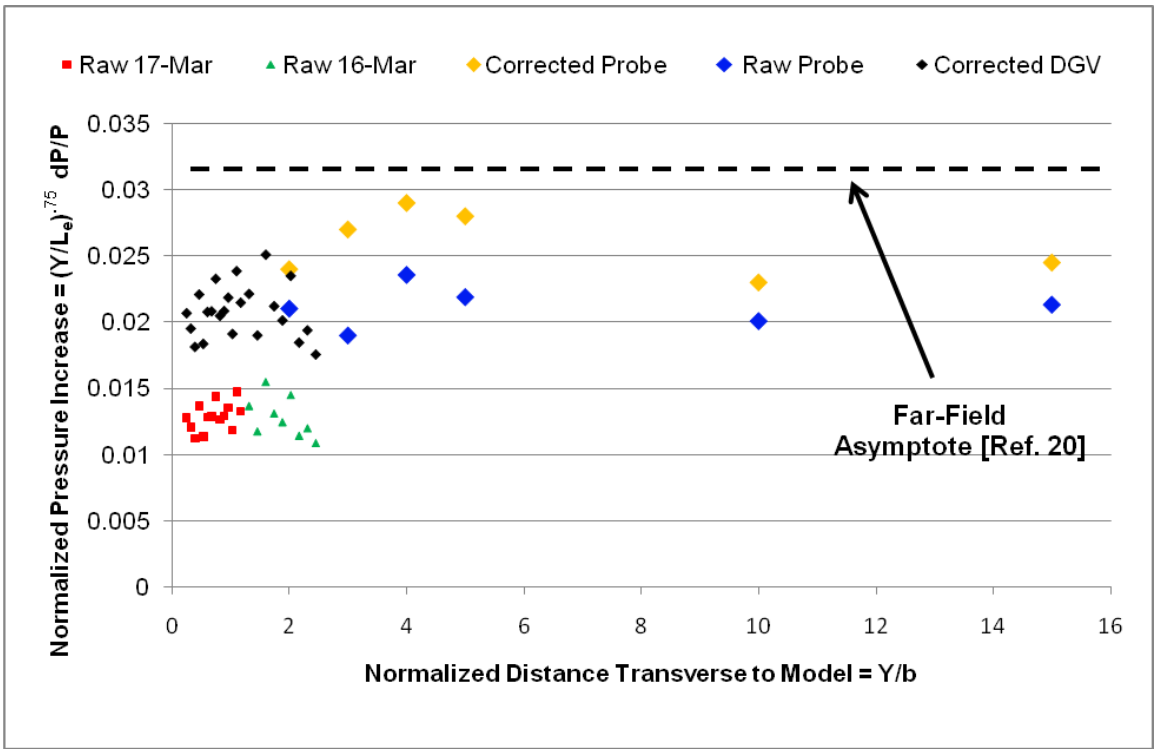

Figure 8 Same data as shown in Figure 7. Both the shock strength (ordinate) and distance downstream (abscissa) have been normalized to reference values to illustrate a constant far field value.

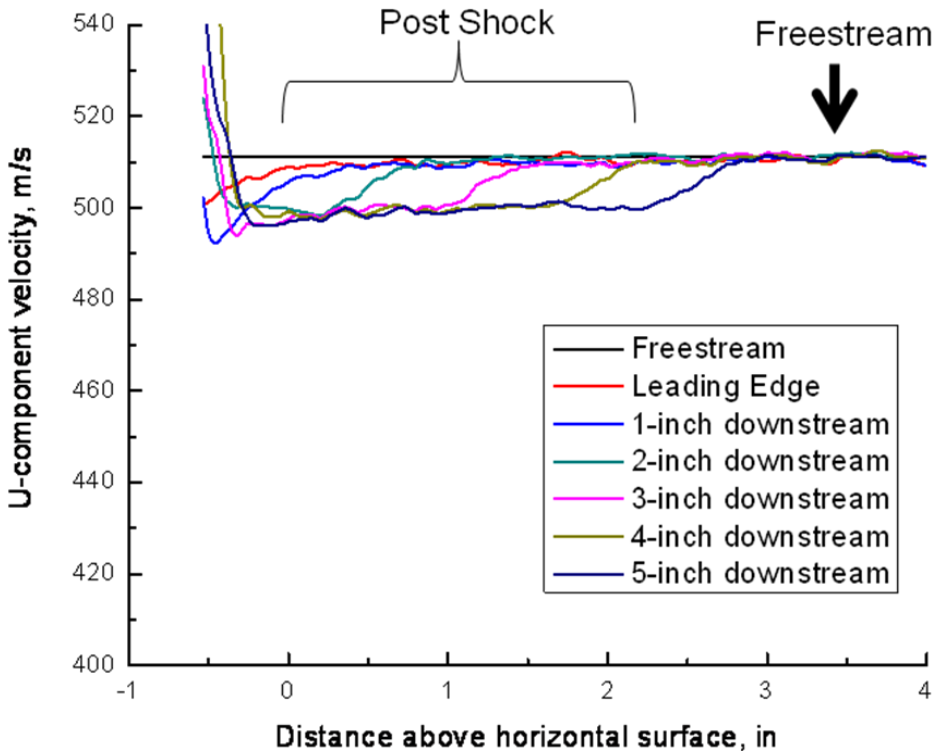

Figure 9 Example of velocity profiles from Reference 7 that were used to determine shock strength across 2-dimensional planar shocks from a flat plate in Reference 7.

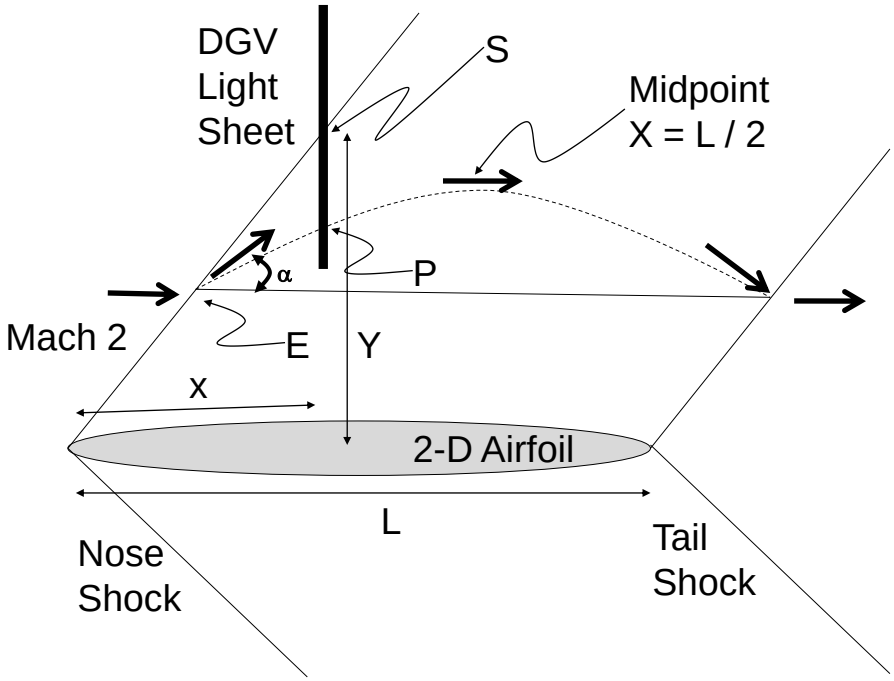

Figure 10 Geometry of typical supersonic flow over a generic lifting slender body.

REPORT DOCUMENTATION PAGE

Form Approved
OMB No. 0704-0188

1. REPORT DATE *(DD-MM-YYYY)*	2. REPORT TYPE	3. DATES COVERED *(From - To)*
01- 02 - 2011	Technical Memorandum	

4. TITLE AND SUBTITLE
Conical Shock-Strength Determination on a Low-Sonic-Boom Aircraft Model by Doppler Global Velocimetry

5a. CONTRACT NUMBER

5b. GRANT NUMBER

5c. PROGRAM ELEMENT NUMBER

6. AUTHOR(S)
Herring, Gregory C.; Meyers, James F.

5d. PROJECT NUMBER

5e. TASK NUMBER

5f. WORK UNIT NUMBER
984754.02.07.07.11.03

7. PERFORMING ORGANIZATION NAME(S) AND ADDRESS(ES)
NASA Langley Research Center
Hampton, VA 23681-2199

8. PERFORMING ORGANIZATION REPORT NUMBER
L-19971

9. SPONSORING/MONITORING AGENCY NAME(S) AND ADDRESS(ES)
National Aeronautics and Space Administration
Washington, DC 20546-0001

10. SPONSOR/MONITOR'S ACRONYM(S)
NASA

11. SPONSOR/MONITOR'S REPORT NUMBER(S)
NASA/TM-2011-217052

12. DISTRIBUTION/AVAILABILITY STATEMENT
Unclassified - Unlimited
Subject Category 74
Availability: NASA CASI (443) 757-5802

13. SUPPLEMENTARY NOTES

14. ABSTRACT

A nonintrusive technique Doppler global velocimetry (DGV) was used to determine conical shock strengths on a supersonic-cruise low-boom aircraft model. The work was performed at approximately Mach 2 in the Unitary Plan Wind Tunnel. Water is added to the wind tunnel flow circuit, generating small ice particles used as seed particles for the laser-based velocimetry. DGV generates two-dimensional (2-D) maps of three components of velocity that span the oblique shock. Shock strength (i.e. fractional pressure increase) is determined from observation of the flow deflection angle across the shock in combination with the standard shock relations. Although DGV had conveniently and accurately determined shock strengths from the homogenous velocity fields behind 2-D planar shocks, the inhomogeneous 3-D velocity fields behind the conical shocks presented additional challenges. Shock strength measurements for the near-field conical nose shock were demonstrated and compared with previously-published static pressure probe data for the same model in the same wind tunnel. Fair agreement was found between the two sets of results.

15. SUBJECT TERMS
Velocity measurement; Supersonic speed; Flow velocity; Doppler global velocimetry; Sonic boom

16. SECURITY CLASSIFICATION OF:			17. LIMITATION OF ABSTRACT	18. NUMBER OF PAGES	19a. NAME OF RESPONSIBLE PERSON
a. REPORT	b. ABSTRACT	c. THIS PAGE			STI Help Desk (email: help@sti.nasa.gov)
					19b. TELEPHONE NUMBER *(Include area code)*
U	U	U	UU	34	(443) 757-5802